The Astrophysical Journal, 959:109 (8pp), 2023 December 20 https://doi.org/10.3847/1538-4357/acfcb2

Scale Invariance in Gamma-Ray Flares of the Sun and 3C 454.3

Fang-Kun Peng[1], Jun-Jie Wei[2,3], and Hai-Qin Wang[1]
[1] Department of Physics, Anhui Normal University, Wuhu 241002, People's Republic of China
[2] Purple Mountain Observatory, Chinese Academy of Sciences, Nanjing 210023, People's Republic of China; jjwei@pmo.ac.cn
[3] School of Astronomy and Space Sciences, University of Science and Technology of China, Hefei 230026, People's Republic of China
Received 2023 August 20; revised 2023 September 20; accepted 2023 September 23; published 2023 December 12

Abstract

Using the gamma-ray flare samples of the Sun and 3C 454.3 observed by the Fermi telescope, we investigate the statistical properties of sizes including fluence (energy), peak flux (luminosity), duration time, and waiting time in this work. We find that the cumulative distribution of the fluctuations of these sizes follow well the Tsallis q-Gaussian function. The obtained q values from q-Gaussian distribution remain stable around 2 without any significant change, implying that there is a scale invariance structure in gamma-ray flares of the Sun and 3C 454.3. This scale invariance characteristics of the Sun and 3C 454.3 indicated by q values are also comparable to those of earthquakes, soft gamma repeaters, fast radio burst (FRB 20121102), and X-ray flares of gamma-ray bursts. On top of that, we verify the relationship between q values and the power-law indices α from the size frequency distributions, which is expressed as $q = (\alpha + 2)/\alpha$. These statistical findings could be well explained within the physical framework of a self-organizing criticality system.

Unified Astronomy Thesaurus concepts: Gamma-rays (637); Solar flares (1496); Quasars (1319); Astrostatistics (1882)

1. Introduction

GeV flares are one of the most fascinating phenomena for astronomical objects of different scales in the Fermi era. Among them, what we are most familiar with is the Sun, which can emit radiation across most of the electromagnetic spectrum up to high-energy gamma-ray photons during its flare states (Ackermann et al. 2012). Fermi-Large Area Telescope (LAT) recently has detected 45 solar GeV flares above 60 MeV in the first catalog covering the past 24th cycle of solar activity (Ajello et al. 2021). The detailed features of gamma-ray emission, such as duration times, peak fluxes, and fluences for all solar GeV flares are presented. It is possible to perform population studies with such a sizable sample (Ajello et al. 2021; Peng et al. 2023b). Outside the Milky Way, active galactic nuclei (AGNs) represent the dominant class of extragalactic gamma-ray sources (Abdollahi et al. 2022). The overwhelming majority of Fermi-detected AGNs are of the blazar type, which hosts relativistic jets that are pointing very close to our line of sight. 3C 454.3, a typical blazar, has undergone multiple violent gamma-ray outbursts after the launch of Fermi (e.g., Ackermann et al. 2010). A giant gamma-ray eruption from 3C 454.3 in 2009 December was detected by Fermi-LAT, which made it the brightest GeV emitter in the sky for over 1 week (Zhang et al. 2018). According to the Fermi-LAT all-sky survey data, Zhang et al. (2018) decomposed 236 temporal components (flares) in 0.1–200 GeV from 2008 August 6 (MJD 54684) to 2016 February 16 (MJD 57434) for 3C 454.3. The total isotropic energy, peak luminosity, peak time, and duration time of each flare are measured by fitting the 1 day binned light curves with Gaussian functions. Two such samples are very interesting for investigating the acceleration process and radiation mechanism of particles to produce gamma-ray emissions of the Sun and 3C 454.3 from a statistical perspective, which have not been clearly understood yet.

Observations show that the size frequency distribution of solar gamma-ray flares is a power-law function in isotropic energy, peak luminosity, and duration time (Peng et al. 2023b), which could be understood well in self-organized criticality (SOC) system (Aschwanden 2012, 2014, 2022). This concept was first established in the seminal paper (Bak et al. 1987) to explain the ubiquitous $1/f$ noise and power-law correlations. Due to some driving forces or local interactions, an SOC system will self-organize to a critical state at which a small instability can trigger a series of avalanche-like events of any scale, resulting in scale-free, fractal-diffusive, and intermittent avalanches with power-law-like size distributions (e.g., Aschwanden et al. 2016). Lu & Hamilton (1991) initially introduced this theory to solar X-ray flares on assumption that the solar coronal magnetic field is in an SOC state to interpret the power-law distribution of peak count rate over 5 orders of magnitude. This discovery facilitated a host of far-reaching applications of the SOC to astrophysical phenomena (Aschwanden 2011; Aschwanden et al. 2016). In particular, after Wang & Dai (2013) explored successfully the statistical results of X-ray flares of gamma-ray bursts (GRBs) within the physical framework of SOC, it was applied quickly in different areas of astrophysics in recent years: GRBs (Yi et al. 2016; Lyu et al. 2020; Wei 2023), fast radio bursts (FRBs; Wang & Yu 2017; Wang & Zhang 2019; Cheng et al. 2020; Lin & Sang 2020; Wang et al. 2021; Wang et al. 2023; Wei et al. 2021), X-ray bursts in binary (Wang et al. 2017; Zhang et al. 2022), Sgr A* (Neilsen et al. 2013; Li et al. 2015; Wang et al. 2015; Yuan et al. 2018), M87 (Wang et al. 2015; Yang et al. 2019), tidal disruption event Swift J1644+57 (Wang et al. 2015), Mrk 421 (Yan et al. 2018), and 3C 454.3 (Zhang et al. 2018, 2020; Peng et al. 2023a).

In addition to the power-law behavior of size frequency distribution and a linear regression fit among SOC parameters

(e.g., Aschwanden 2012; Peng et al. 2023a), there is a scale-invariance structure in the avalanche size differences, a third SOC hallmark that could be tested easily by observation. Caruso et al. (2007) discovered that the probability density functions (PDFs) of the release energies for the real earthquakes catalogs at different time intervals show a Tsallis q-Gaussian shape, a standard distribution of non-extensive statistical mechanics (Tsallis 1988; Tsallis et al. 1998). The results concerning Tsallis q-statistics reveal the structure of scale invariance for seismic events in the North Aegean area (Iliopoulos et al. 2012). When the different styles of earthquake faulting processes are considered, although the q values vary systematically, it is found that the q-Gaussian distributions with steady q for each faulting type still exist (Wang et al. 2015). In addition, diverse solar activities, sunspots, and solar wind speed fluctuations show clearly non-extensive statistical characters (e.g., Burlaga & Viñas 2004; Pavlos et al. 2012). Since solar flares follow the same energy distribution, the universal properties in solar flare and earthquake dynamics arise naturally in the framework of Tsallis statistical mechanics (e.g., Balasis et al. 2011a, 2011b), implying a common approach to the interpretation of these different phenomena in terms of driving physical mechanisms that have the same feature.

Starquakes frequently happen on a normal neutron star or a magnetar. The crust is locked together with the magnetic field so that any change in one affects the other in all neutron stars. Deformations and cracks in the crusts of neutron stars have been linked with phenomena such as bursts in gamma rays, X-rays, and radio bands. Chang et al. (2017) ascertained that the PDFs of fluctuations of fluences, peak fluxes, and duration times were fitted well with q-Gaussian models for the soft gamma repeater (SGR) J1550-5418, and the obtained best-fit values of q keep approximately constant for different time interval scales. The analogous results were later confirmed in two other SGRs: SGR 1806-20 and SGR J1935+2154 (Wei et al. 2021; Sang & Lin 2022), implying a common scale-invariance feature for X-ray/gamma-ray emission of SGRs. SGR J1935+2154 is well known to associate with a bright Galactic FRB (Mereghetti et al. 2020; Li et al. 2021; Ridnaia et al. 2021; Tavani et al. 2021), which strongly evidences that magnetar engines can produce at least some FRBs. Lin & Sang (2020) investigated the statistical properties of the repeating FRB 121102 with early detections consisting of dozens bursts and showed that the fluctuations of the fluences and energies well follow the the q-Gaussian distribution. Such findings were verified with a larger sample observed by the Five-hundred-meter Aperture Spherical Radio Telescope (FAST; Li et al. 2021; Wei et al. 2021; Du et al. 2023), reflecting a self-similarity structure in the intensity of the temporal occurrence of repeating FRBs. A steady value $q \sim 2$ in q-Gaussian function independent of the temporal interval scale was also revealed in the study on one-off FRBs (Wang et al. 2023). What's more, the relationship between the power-law index α of the size frequency distribution and the q value from Tsallis q-Gaussian model has been investigated in Caruso et al. (2007). On the assumption that there is no correlation between the sizes of the two events, a verifiable expression was analytically obtained straightforwardly in Celikoglu et al. (2010), that is $q = (\alpha + 2)/\alpha$. The q–α relationship was confirmed recently with a GRB X-ray flare sample observed by Swift (Wei 2023). These studies not only mean that the SOC model is self-consistent but also make the q parameter estimated a priori from the known power-law index α of the system (Wei 2023).

The statistical power-law frequency distributions and correlations of observable parameters of gamma-ray flares of the Sun and 3C 454.3 have been explored in Peng et al. (2023a, 2023b). However, their scale-invariance characteristics have not been investigated yet. In fact, to our knowledge, such scale-invariance analysis has not been studied previously with GeV photons to date. In this work, we therefore extend such research to GeV emission with the first solar gamma-ray flare catalog (Ajello et al. 2021) and 236 GeV flares of 3C 454.3 (Zhang et al. 2018). For the total 45 solar GeV flares with a detection significance of $\geqslant 5\sigma$ in the first catalog, we exclude Fermi-LAT low-energy flares only and just focus on the subsample selected with the standard analysis pipeline; see Table 1 in Ajello et al. (2021). The final sample chosen for our analysis thus contains 39 solar GeV flares. On one hand, it is interesting to check if flares at the GeV band from the Sun and the jet around the supermassive black hole system share the same pattern in scale invariance as earthquakes, SGRs, FRBs, and GRBs or not. On the other hand, we try to examine if the above-mentioned relationship between the power-law index α and the q parameter still holds for GeV flares of these two sources. The rest of this paper is organized as follows. The data analysis and fitting method are presented in Section 2. In Section 3, we make the scale-invariance analyses on fluence (energy), peak flux (luminosity), duration time, and waiting time of the Sun and 3C 454.3, respectively. Finally, discussion and conclusion are given in Section 4.

2. Method

Based on the all-sky survey data collected by Fermi-LAT (Zhang et al. 2018; Ajello et al. 2021), we carry on the scale-invariance analysis following the threads in previous work (e.g., Wei 2023). Since the spectral energy distribution of each solar GeV flare is not available, we use the total fluence (in unit of photons per centimeters squared) and peak flux (in units of photons per centimeters squared per second) to represent the total energy and peak luminosity, respectively. The duration times are from the fifth column (named as total duration) in Table 1 of Ajello et al. (2021). The waiting time is defined as the time difference between two subsequent flare events. It is difficult to identify the exact starting dates and ending dates of the Fermi-LAT solar flares due to LAT data gap or low statistic not sufficient to perform a fine time-binning analysis (Ajello et al. 2021). All the cases of solar gamma-ray flares are accompanied by a specific Geostationary Operational Environmental Satellite (GOES) observation. The mean of the duration time of GOES flares is 0.9 hr, which is shorter than that of Fermi-LAT flares (4.3 hr). Both timescales are much smaller than the averaged interval ~63 days of waiting times for solar GeV flares. For simplicity, we just construct roughly the waiting time from the difference of the starting time detected by GOES, i.e., shown in column 3 of Table 1 from Ajello et al. (2021). We check the definition of waiting time from the difference of the ending time detected by GOES, and no statistical difference is found as well.

For solar GeV flares, we pay attention to the fluctuations of sizes, including fluence, peak flux, duration time, and waiting time. X_j is the jth size from the observation directly in time order. Obviously, the minimum and maximum values of j are 1 and the total number of gamma-ray flares N, here $N = 39$. The

corresponding size differences are defined as $x_n = X_{j+n} - X_j$, where n is an arbitrary integer and indicates the temporal interval scale. Generally, the dimensionless size fluctuation, namely $\{z_n = x_n/\sigma\}$, is usually used to study the scale-invariance property, where σ means the standard deviation of data set $\{x_n\}$.

The size fluctuation distributions of earthquakes, SGRs, FRB 20121102, and X-ray flares of GRBs could be fitted well with a Tsallis q-Gaussian model (Caruso et al. 2007; Wang et al. 2015; Chang et al. 2017; Lin & Sang 2020; Wei et al. 2021; Sang & Lin 2022; Wei 2023). The Tsallis q-Gaussian function is written as (Tsallis 1988; Tsallis et al. 1998)

$$f(z_n) = A[1 - B(1 - q)z_n^2]^{(1/(1-q))}, \quad (1)$$

where A is the prefactor, B is the width of the distribution, and q determines the sharpness. Among these parameters q demonstrates the difference between Tsallis q-Gaussian and common Gaussian function. Compared to the common Gaussian distribution, the q-Gaussian distribution shows a sharp peak and a long-tailed tendency when q is greater than 1. One can see that when q gets close to 1, the above q-Gaussian function will reduce to a common Gaussian distribution with mean of 0 and standard deviation $\sigma = 1/\sqrt{2B}$. Considering that only some dozens of GeV flares are available for the Sun (Ajello et al. 2021), we use the cumulative distribution function (CDF) of q-Gaussian to fit the observational data

$$F(z_n) = \int_{-\infty}^{z_n} f(z_n)dz_n. \quad (2)$$

For a specific n, the parameters of A, B, and q from the Tsallis q-Gaussian model would be constrained simultaneously by minimizing the χ^2 statistic, which can be formulated as

$$\chi^2 = \sum_{i=1}^{N-n} \frac{[N_{\rm cum}(\leqslant z_{n,i}) - F(z_{n,i})]^2}{\sigma_{{\rm cum},i}^2}, \quad (3)$$

where $N_{\rm cum}(\leqslant z_{n,i}) = i$ is the observed event number in rescaled size differences, with the corresponding uncertainty $\sigma_{{\rm cum},i} = \sqrt{N_{\rm cum}(\leqslant z_{n,i})}$. The total number of data set $\{z_{n,i}\}$ is $(N - n)$ for a fixed n. We then use the Python Markov Chain Monte Carlo (MCMC) module EMCEE (Foreman-Mackey et al. 2013) to determine the errors from the posterior distributions of model parameters. Since the priors are not important when sampling enough samples with the MCMC method, we take the priors of all the parameters as uniform distributions in a relatively large range. That is to say, we set prior distributions for model parameters as $\log_{10}A \in [-2, 8]$, $\log_{10}B \in [-2, 8]$, and $q \in [1, 1000]$, respectively, during the fitting.

3. Scale Invariance in GeV Flares

The data set could be well depicted by Equation (2) for the differences of the fluences, peak fluxes, duration times, and waiting times of solar GeV flares. Figure 1 exhibits CDFs of the differences for fluences (top left panel), peak fluxes (top right panel), duration times (bottom left panel), and waiting times (bottom right panel), respectively. Here circles, crosses, and stars denote cases of $n = 1$, $n = 8$, and $n = 15$, respectively. The solid lines show the best-fitting models with q-Gaussian function. The uncertainties of the data points are not shown in this figure for clarity. Most data points are noticeably distributed around 0, and there are few observations toward the two tails of the distribution. The large fluctuations appearing in both tails are caused by the incompleteness, which are given from the absence of sampling of small magnitude events at the global scale. These facts mean that there are rare but large fluctuations, and small fluctuations are most likely to happen. The best-fitting results of q values are listed in Table 1. One can see that q values are approximately constant without any significant change. We further calculate CDFs of sizes differences by taking more different scale intervals into consideration, namely $1 \leqslant n \leqslant 15$, and fit the CDFs with q-Gaussian function. It is found that q values are distributed within a very narrow range and could be almost treated as a constant independent of n; see Figure 3 (left panel) for more details, where the shaded regions mark the 1σ deviation. The mean values of q for fluence, peak flux, duration time, and waiting time of solar GeV flares are 2.38 ± 0.12, 2.45 ± 0.15, 1.90 ± 0.20, and 1.86 ± 0.26, respectively, which are listed in Table 2 and calculated as follows. q_n is the central value of the best-fitting result of q when a specific n is adopted. For all different scale intervals, we could obtain the data array of $\{q_1, q_2...q_8...q_{14}, q_{15}\}$. Based on the above data array, we can estimate the mean and error values of q. The uncertainties represent the 1σ standard deviation of q values. All quoted uncertainties are 1σ (i.e., 68%) confidence intervals unless otherwise stated throughout this article.

Table 1
The Best-fitting q Values in the q-Gaussian Model for the Sun and 3C 454.3

Source	Parameters	$n = 1$	$n = 8$	$n = 15$
The Sun	q-fluence	$2.53^{+0.14}_{-0.17}$	$2.41^{+0.21}_{-0.26}$	$2.18^{+0.28}_{-0.39}$
	q-peak Flux	$2.63^{+0.12}_{-0.14}$	$2.50^{+0.21}_{-0.27}$	$2.28^{+0.32}_{-0.57}$
	q-duration	$1.91^{+0.22}_{-0.23}$	$1.66^{+0.39}_{-0.40}$	$1.90^{+0.45}_{-0.44}$
	q-waiting Time	$1.83^{+0.32}_{-0.41}$	$1.28^{+0.29}_{-0.19}$	$2.06^{+0.44}_{-0.56}$
		$n = 1$	$n = 20$	$n = 40$
3C 454.3	q-energy	$1.92^{+0.04}_{-0.04}$	$2.00^{+0.04}_{-0.04}$	$2.10^{+0.04}_{-0.04}$
	q-peak Luminosity	$1.98^{+0.03}_{-0.03}$	$2.00^{+0.03}_{-0.03}$	$1.96^{+0.04}_{-0.04}$
	q-duration	$1.76^{+0.04}_{-0.04}$	$1.81^{+0.04}_{-0.04}$	$1.70^{+0.05}_{-0.05}$
	q-waiting Time	$2.02^{+0.03}_{-0.03}$	$1.95^{+0.04}_{-0.04}$	$1.92^{+0.04}_{-0.04}$

For 236 gamma-ray flares of 3C 454.3 (Zhang et al. 2018), we also make a similar analysis. Figure 2 displays three examples of observation data and best-fitting models. We show in this figure the cumulative distributions of the differences of isotropic gamma-ray energies (top left panel), peak luminosities (top right panel), duration times (bottom left panel), and waiting times (bottom right panel) for the temporal interval scale $n = 1$ (circles), $n = 20$ (crosses), and $n = 40$ (stars), respectively. The blue, red, and green smooth curves exhibit the q-Gaussian model functions for $n = 1$, $n = 20$, and $n = 40$, respectively. The best-fitting q values and their uncertainties for $n = 1$, 20, 40 are listed in Table 1. When the rescaled cumulative distributions of the size distributions at different temporal intervals are analyzed ($1 \leqslant n \leqslant 40$), then we see that the data points representing results for each size in Figure 3 (right panel) are almost independent of n. The mean values of q for isotropic energy, peak luminosity, duration time, and waiting time are 2.05 ± 0.05, 1.97 ± 0.04, 1.77 ± 0.07, and 1.94 ± 0.06, respectively, which are shown in Table 2. Since the sample size is relatively large, we check the results with a

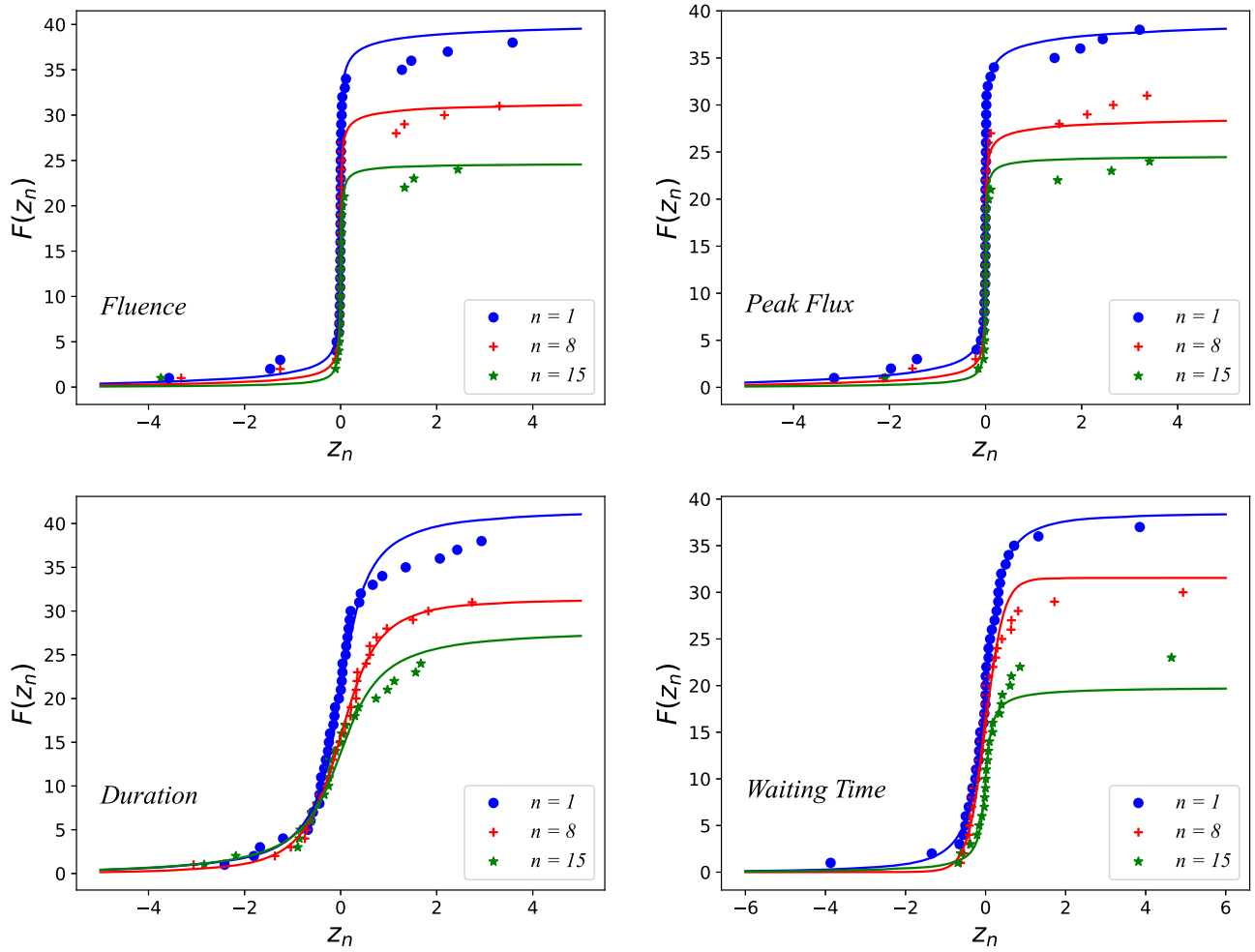

Figure 1. Scale-invariance structure of solar GeV flares. Cumulative distributions with q-Gaussian function (solid lines) for the differences of fluences (upper left panel), peak fluxes (upper right panel), duration times (lower left panel), and waiting times (lower right panel) for $n = 1$ (circles), $n = 8$ (crosses), and $n = 15$ (stars), respectively.

Table 2
The Mean Values of q in the q-Gaussian Distribution for the Sun and 3C 454.3

Source	Number	q-energy	q-peak Luminosity	q-duration	q-waiting Time	References
The Sun	39	2.38 ± 0.12	2.45 ± 0.15	1.90 ± 0.20	1.86 ± 0.26	This work
3C 454.3	236	2.05 ± 0.05	1.97 ± 0.04	1.77 ± 0.07	1.94 ± 0.06	This work
Earthquakes	400,000	1.75 ± 0.15	...	...	...	Caruso et al. (2007)
SGR J1550-5418	384	2.41 ± 0.29	2.40 ± 0.30	2.06 ± 0.23	$\sim$1.00	Chang et al. (2017)
SGR 1806-20	924	2.72 ± 0.05	2.65 ± 0.05	2.48 ± 0.05	...	Wei et al. (2021)
SGR J1935+2154	260	2.78 ± 0.12	...	2.28 ± 0.15	...	Wei et al. (2021)
FRB 121102	1652[a]	2.51 ± 0.03	2.50 ± 0.03	1.42 ± 0.04	...	Wei et al. (2021)
	1253[b]	1.63 ± 0.09	1.81 ± 0.05	1.39 ± 0.06	...	Wei et al. (2021)
	399[b]	2.21 ± 0.10	2.34 ± 0.09	1.50 ± 0.16	...	Wei et al. (2021)
X-Ray flares	200	2.22 ± 0.10	...	2.57 ± 0.04	2.37 ± 0.04	Wei (2023)

Notes. For comparison, q values measured from earthquakes, SGRs, FRB 121102, and X-ray flares of GRBs are listed.
[a] The overall 1652 bursts of FRB 121102 detected by FAST (Li et al. 2021).
[b] The 1253 low-energy bursts with energies $\leqslant 2 \times 10^{38}$ erg, and high-energy bursts with energies $>2 \times 10^{38}$ erg, respectively.

larger time interval $n = 60$, 80, 100, and 120; the best-fitting q values are consistent with the above mean values within 2σ error. Compared to the results of the Sun, the uncertainties of q of those of 3C 454.3 are relatively smaller, possibly due to a larger sample number of gamma-ray flares, which in turn leads to relatively small statistical errors.

During the process, we note that the q values would contain 1 within errors for scale-invariance analysis of solar GeV flares on waiting time in some cases, implying that these fluctuations maybe tend to a Gaussian distribution. Chang et al. (2017) revealed that the q values of q-Gaussian function that fit the fluctuations of waiting time at different intervals approach 1 for

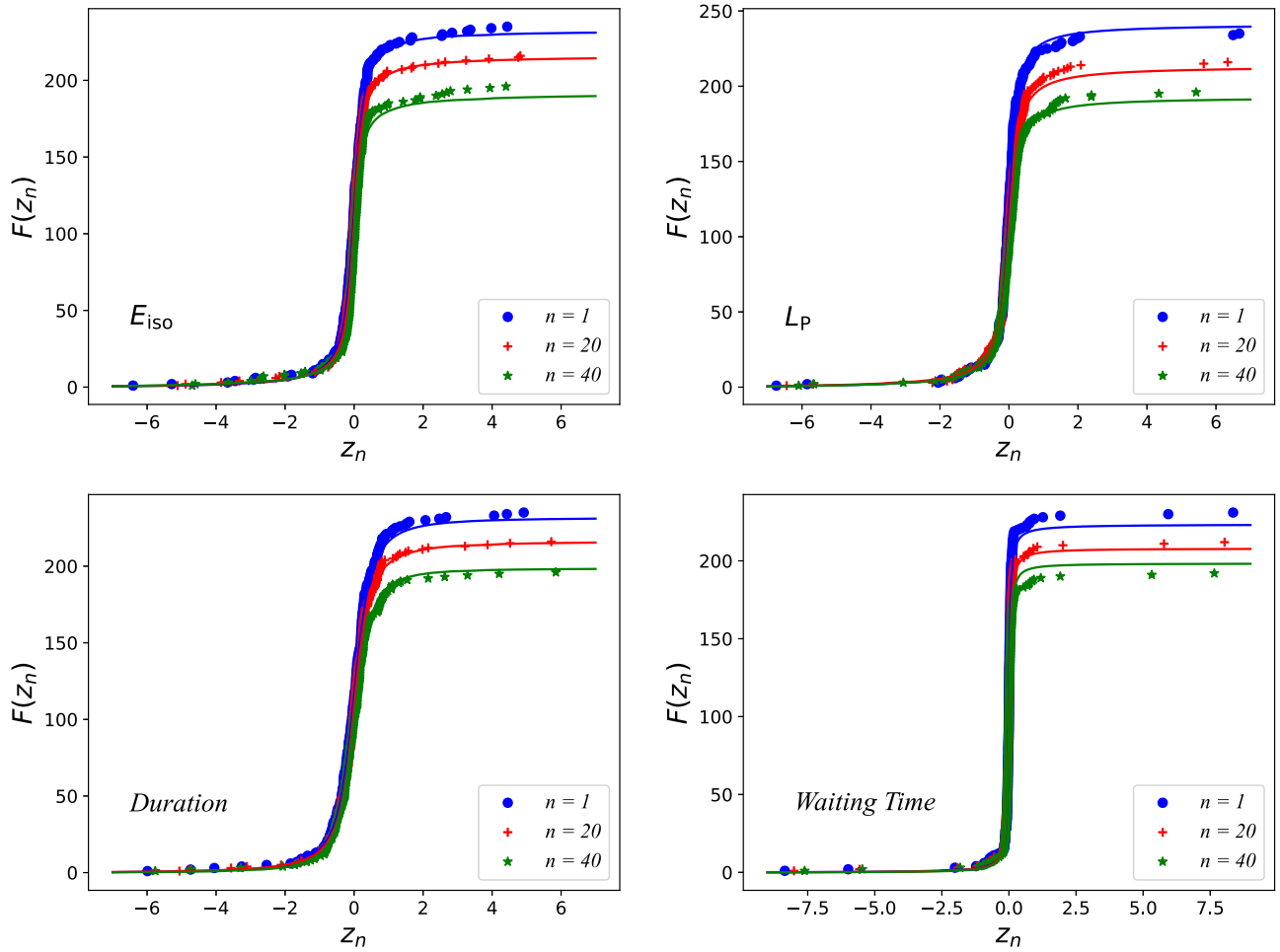

Figure 2. Scale-invariance structure of gamma-ray flares of 3C 454.3. Cumulative distributions with q-Gaussian function (solid lines) for the differences of isotropic gamma-ray energies ($E_{\rm iso}$, upper left panel), peak luminosities ($L_{\rm P}$, upper right panel), duration times (lower left panel), and waiting times (lower right panel) for $n = 1$ (circles), $n = 20$ (crosses), and $n = 40$ (stars), respectively.

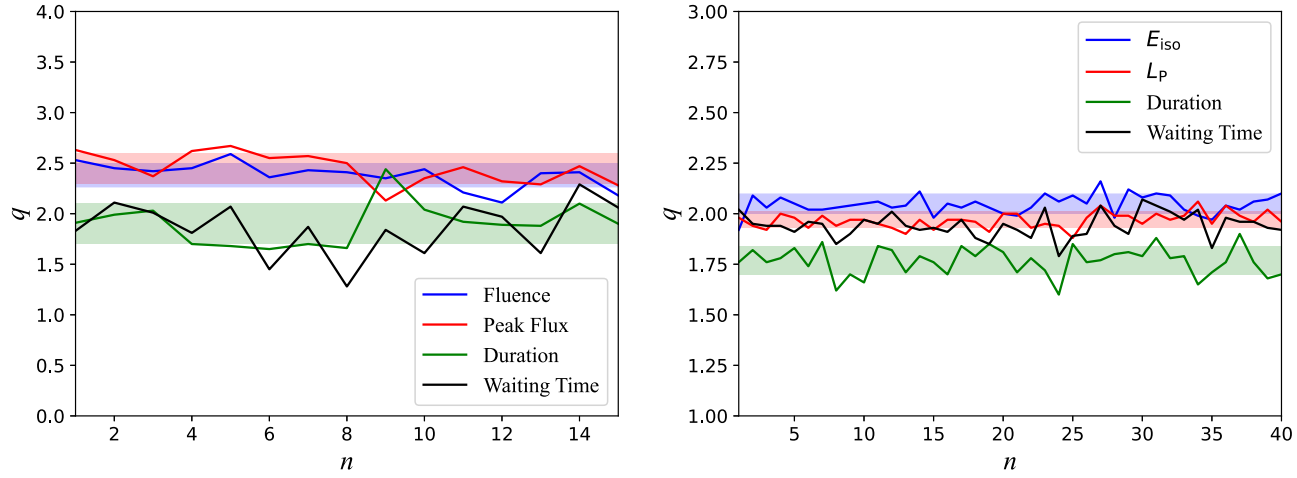

Figure 3. The best-fitting q values from Equation (1) with 1σ regions (shaded) as a function of n for gamma-ray flares of the Sun (left panel) and 3C 454.3 (right panel), respectively. The uncertainties of q values for waiting time are not shown for clarity.

SGR J1550-5418. Similar scenarios have been also found in FRB 20121102 (Lin & Sang 2020; Wei et al. 2021). For solar GeV flares, when n takes 8 and 10, the q-Gaussian function did not fit the CDFs of waiting time differences very well, and q values are not effectively constrained. There are two possible reasons. One is the small sample size of solar GeV flares, the other is the possible intrinsic difference between waiting time and other sizes. For example, in the case of FRB 20121102, the waiting time shows a complex distribution and could be fitted by two or three log-normal functions, which is consistent with a stochastic process of the central engine (e.g., Li et al. 2021). Comprehensive analysis on the coherent growth in the burst

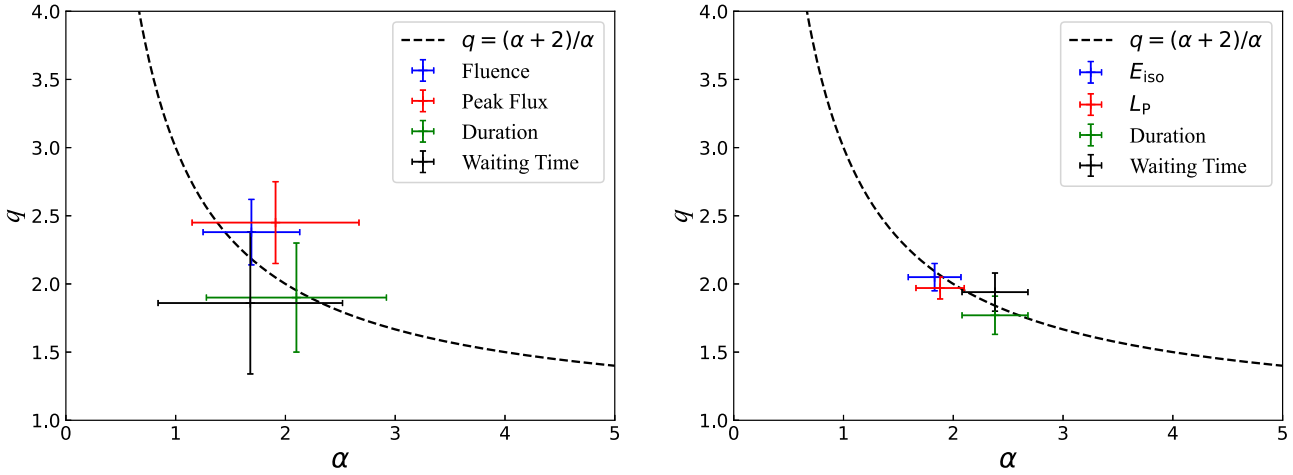

Figure 4. The relationship between parameters q (from the q-Gaussian function) and α (from the size frequency distribution) for gamma-ray flares of the Sun (left panel) and 3C 454.3 (right panel), respectively. The dashed line shows the predicted curves from Equation (4). Data points with 2σ error bars correspond to the best-fitting values of q and α estimated for the energies (blue dot), peak luminosities (red dot), duration times (green dot), and waiting times (black dot), respectively.

time structures and the Hurst exponent indicates that FRB 20121102 discloses memory from minutes to hour, which supports that the triggers of bursts are correlated (Wang et al. 2023). More solar gamma-ray flares detected in the future would shine a light on this issue.

Fermi satellite is a low-orbit instrument; data gaps seem inevitable resulting from the shadow of the Earth or irregular switch on/off periods during some parts of the orbit, such as when the spacecraft passes through the South Atlantic Anomaly. At the same time, the resolution of gamma-ray flares is usually related with the detector sensitivity or background definition, which would result in undersampling below the detection threshold, and hence, show a deviation from an ideal power-law function of frequency distribution of the sizes (Aschwanden 2015). However, in contrast to the fact that the lower end of the size frequency distribution is often subject to incomplete sampling, the size fluctuations have a common structure, i.e., nearly constant q values at different scale intervals, as shown in Figure 3. This points to the fact that the research on scale invariance is weakly sensitive to the weak events below the Fermi-LAT detection threshold or absence of continuous observation. The scale-invariance analysis, presented by the q-Gaussian function, suggests a new, powerful, and robust way for characterizing the presence of criticality or scale-free structure in a system.

4. Discussion and Conclusion

These statistical results support a common scale-invariance structure of gamma-ray flares from the Sun and 3C 454.3. Magnetic reconnection driving solar flares is widely accepted from theories and observations, so magnetic dissipation process is the most likely mechanism to account for gamma-ray emission in jets of 3C 454.3 (Peng et al. 2023a, 2023b). Theoretically, the magnetic field energy is calculated with multiwavelength observations in a conventional one-zone leptonic model, which indicate a magnetically dominated jet for 3C 454.3 (e.g., Zhang et al. 2014; Tan et al. 2020). Kadowaki et al. (2015) compare different fast magnetic reconnection triggering mechanisms and find that the gamma-ray emission can be due to magnetic power released involving fast reconnection derived by turbulence for a large sample of AGNs (including 3C 454.3).

In general, for the real earthquakes, it is well known that the avalanche size (energy) S occurs with a power-law distribution $p(S) \sim S^{-\alpha}$. Caruso et al. (2007) discovered that the size difference ($z = S(t + \Delta) - S(t)$) distributions appear to have the form of q-Gaussian. The accurate relationship relating α values and q values cloud be explicitly estimated in some models (Caruso et al. 2007; Celikoglu et al. 2010). To find the mathematical derivation, one should consider the following two assumptions. One is the power-law size distribution, and the other hypothesis is that the process of avalanches is independent. The expression of the distribution of the difference $p(z)$ cloud be explicitly derived as Equation (3) in Celikoglu et al. (2010). After simplification and approximation, one finally has $p(z) \sim |z|^{-\alpha} (z \gg 1)$. Compared with the q-Gaussian function, the theoretical relationship between the power-law index α from the size frequency distribution and the q value from the size differences could be straightforwardly obtained as Equation (5) in Celikoglu et al. (2010):

$$q = \frac{2 + \alpha}{\alpha}. \quad (4)$$

Using the average q values from Table 2 and the best-fitting power-law indices α from the size frequency distributions in previous works (Peng et al. 2023a, 2023b) for gamma-ray flares of the Sun and 3C 454.3, now we will check the relationship of Equation (4). The estimated α and q values for fluence (energy), peak flux (luminosity), duration time, and waiting time of the Sun (3C 454.3) are shown as blue, red, green, and black dots in Figure 4. One can see that our results are consistent with the theoretical prediction of Equation (4) within 2 standard deviations. These results, self-consistent with previous findings, confirm that the process producing the gamma-ray flares of the Sun and 3C 454.3 is at a similar SOC state.

At first glance, q values obtained from different objects (including earthquakes, SGRs, FRB 20121102, and GRB X-ray flares) look comparable within error bars, as shown in Table 2. Wang et al. (2015) investigated the PDFs of energy fluctuations with tens of thousands of event samples for different faulting styles and compared them with q-Gaussian functions. It was found that the q values are different clearly for the normal (q_N),

strike-slip (q_{SS}), and thrust (q_T) events: $q_N \lesssim q_{SS} \lesssim q_T$, which hints that q values could cast a light on the microdynamic process of the earthquake system. Inspired by this, if we move the focus to the central values of q, we find that the q values for fluence, peak flux, duration time, and waiting time of the Sun are somewhat different from those of 3C 454.3. Different q values reflect different α values, which connect the fractal dimension directly in the fractal-diffusive SOC system (Aschwanden 2012, 2014, 2022). In the Olami–Feder–Christensen earthquake model established by Olami et al. (1992), the exponent value α from the power-law distribution of the avalanche size (also the q value from size fluctuation) varies with the different levels of the system conservation, an inherent parameter that is determined by the relative value of the relevant elastic parameters describing the model. Additionally, the waiting time distribution is characterized as a nonstationary Poisson process in the SOC system (Aschwanden & McTiernan 2010). If we assume various event rates $\lambda(t)$, parameterized with power-law function as follows $\lambda(t) \propto t^{\gamma}$, one could derive an analytical solution of the waiting time distribution for different γ, that is, a power-law function with slope $(2 + 1/\gamma)$ (Wang et al. 2017; Aschwanden et al. 2021). Therefore, the q values of waiting time difference distribution would relate with the flare event rate as well, and the scale-invariance structure in waiting time provides a new means to diagnose the form of event rate. In terms of center value, the q values are slightly different for the Sun and 3C 454.3. If the statistical differences between the Sun and 3C 454.3 are confirmed by future observations, on one hand, it implies that some underlying microphysics controlling the SOC process but without well understanding are different for these two objects. On the other hand, we should pay attention to the extension study with concepts from the Sun to other systems.

In conclusion, based on the Fermi-LAT survey data, we study the different distribution properties of gamma-ray flares from the Sun and blazar 3C 454.3. It is found that the CDFs of the differences of energies, peak luminosities, duration times, and waiting times could be modeled well with a Tsallis q-Gaussian function, which is the standard distribution in non-extensive statistical mechanics. The obtained q values keep approximately constant when different time intervals are adopted. Combined with previous outcomes on size frequency distribution, denoted as α, we test the relationship between α values and q values for energy, peak luminosity, duration time, and waiting time of the Sun and 3C 454.3 and find that the data points locate on the theoretical prediction curves. The obtained q values are not only comparable for the Sun and 3C 454.3 but also in line with the results of the earthquakes, SGRs, FRB 20121102, and X-ray flares of GRBs within error bars. These findings indicate that gamma-ray flares from the Sun and 3C 454.3 show a common scale-invariant property. The q-Gaussian distribution is argued to be an important component in describing the presence of criticality in a system; our results support that the energy dissipation mechanism responsible for gamma-ray flares of the Sun and 3C 454.3 might be at a similar SOC state, such as magnetic reconnection usually mentioned in solar physics. We thus suggest that magnetic energy stored inside the large-scale jet and released through turbulence-driven reconnection is the source of acceleration of electrons and ions to relativistic energies for 3C 454.3.

Acknowledgments

We thank the anonymous referees for useful comments and suggestions. We are grateful to F. Y. Wang and H. P. Chen for useful discussions. This work is partially supported by the National Key Research and Development Program of China (grant Nos. 2022SKA0130101 and 2022SKA0130102), the National Natural Science Foundation of China (grants Nos. 12003002, 12373053, 12321003, and 12041306), the Key Research Program of Frontier Sciences (grant No. ZDBS-LY-7014) of Chinese Academy of Sciences, the Natural Science Foundation of Jiangsu Province (grant No. BK20221562), and the Young Elite Scientists Sponsorship Program of Jiangsu Association for Science and Technology. F.K.P. also acknowledges support from the University Annual Scientific Research Plan of Anhui Province 2023 (2023AH050146), the Excellent Teacher Training Program of Anhui Province (2023), and the Doctoral Starting up Foundation of Anhui Normal University 2020 (903/752022).

ORCID iDs

Fang-Kun Peng https://orcid.org/0000-0001-7171-5132
Jun-Jie Wei https://orcid.org/0000-0003-0162-2488

References

Abdollahi, S., Acero, F., Baldini, L., et al. 2022, ApJS, 260, 53
Ackermann, M., Ajello, M., Allafort, A., et al. 2012, ApJ, 745, 144
Ackermann, M., Ajello, M., Baldini, L., et al. 2010, ApJ, 721, 1383
Ajello, M., Baldini, L., Bastieri, D., et al. 2021, ApJS, 252, 13
Aschwanden, M. J. 2011, Self-Organized Criticality in Astrophysics (Berlin: Springer)
Aschwanden, M. J. 2012, A&A, 539, A2
Aschwanden, M. J. 2014, ApJ, 782, 54
Aschwanden, M. J. 2015, ApJ, 814, 19
Aschwanden, M. J. 2022, ApJ, 934, 33
Aschwanden, M. J., Crosby, N. B., Dimitropoulou, M., et al. 2016, SSRv, 198, 47
Aschwanden, M. J., Johnson, J. R., & Nurhan, Y. I. 2021, ApJ, 921, 166
Aschwanden, M. J., & McTiernan, J. M. 2010, ApJ, 717, 683
Bak, P., Tang, C., & Wiesenfeld, K. 1987, PhRvL, 59, 381
Balasis, G., Daglis, I. A., Anastasiadis, A., et al. 2011a, PhyA, 390, 341
Balasis, G., Daglis, I. A., Papadimitriou, C., et al. 2011b, Entrp, 13, 1865
Burlaga, L. F., & Viñas, A. F. 2004, GeoRL, 31, L16807
Caruso, F., Pluchino, A., Latora, V., Vinciguerra, S., & Rapisarda, A. 2007, PhRvE, 75, 055101
Celikoglu, A., Tirnakli, U., & Queirós, S. M. D. 2010, PhRvE, 82, 021124
Chang, Z., Lin, H.-N., Sang, Y., & Wang, P. 2017, ChPhC, 41, 065104
Cheng, Y., Zhang, G. Q., & Wang, F. Y. 2020, MNRAS, 491, 1498
Du, Y., Wang, P., Song, L., & Xiong, S. 2023, arXiv:2305.04738
Foreman-Mackey, D., Hogg, D. W., Lang, D., & Goodman, J. 2013, PASP, 125, 306
Iliopoulos, A. C., Pavlos, G. P., Papadimitriou, E. E., et al. 2012, IJBC, 22, 1250224
Kadowaki, L. H. S., de Gouveia Dal Pino, E. M., & Singh, C. B. 2015, ApJ, 802, 113
Li, C. K., Lin, L., Xiong, S. L., et al. 2021, NatAs, 5, 378
Li, D., Wang, P., Zhu, W. W., et al. 2021, Natur, 598, 267
Li, Y.-P., Yuan, F., Yuan, Q., et al. 2015, ApJ, 810, 19
Lin, H.-N., & Sang, Y. 2020, MNRAS, 491, 2156
Lu, E. T., & Hamilton, R. J. 1991, ApJL, 380, L89
Lyu, F., Li, Y.-P., Hou, S.-J., et al. 2020, FrPhy, 16, 14501
Mereghetti, S., Savchenko, V., Ferrigno, C., et al. 2020, ApJL, 898, L29
Neilsen, J., Nowak, M. A., Gammie, C., et al. 2013, ApJ, 774, 42
Olami, Z., Feder, H. J. S., & Christensen, K. 1992, PhRvL, 68, 1244
Pavlos, G. P., Karakatsanis, L. P., & Xenakis, M. N. 2012, PhyA, 391, 6287
Peng, F.-K., Hou, S.-J., Zhang, H.-M., Xue, R., & Shu, X.-W. 2023a, MNRAS, 520, 5974
Peng, F.-K., Wang, F.-Y., Shu, X.-W., & Hou, S.-J. 2023b, MNRAS, 518, 3959
Ridnaia, A., Svinkin, D., Frederiks, D., et al. 2021, NatAs, 5, 372

Sang, Y., & Lin, H.-N. 2022, MNRAS, 510, 1801
Tan, C., Xue, R., Du, L.-M., et al. 2020, ApJS, 248, 27
Tavani, M., Casentini, C., Ursi, A., et al. 2021, NatAs, 5, 401
Tsallis, C. 1988, JSP, 52, 479
Tsallis, C., Mendes, R., & Plastino, A. R. 1998, PhyA, 261, 534
Wang, F. Y., & Dai, Z. G. 2013, NatPh, 9, 465
Wang, F. Y., Dai, Z. G., Yi, S. X., & Xi, S. Q. 2015, ApJS, 216, 8
Wang, F. Y., Wu, Q., & Dai, Z. G. 2023, ApJL, 949, L33
Wang, F. Y., & Yu, H. 2017, JCAP, 03, 023
Wang, F. Y., & Zhang, G. Q. 2019, ApJ, 882, 108
Wang, F. Y., Zhang, G. Q., & Dai, Z. G. 2021, MNRAS, 501, 3155
Wang, J. S., Wang, F. Y., & Dai, Z. G. 2017, MNRAS, 471, 2517
Wang, P., Chang, Z., Wang, H., & Lu, H. 2015, EPJB, 88, 206
Wang, Z.-H., Sang, Y., & Zhang, X. 2023, RAA, 23, 025002
Wei, J.-J. 2023, PhRvR, 5, 013019
Wei, J.-J., Wu, X.-F., Dai, Z.-G., et al. 2021, ApJ, 920, 153
Yan, D., Yang, S., Zhang, P., et al. 2018, ApJ, 864, 164
Yang, S., Yan, D., Dai, B., et al. 2019, MNRAS, 489, 2685
Yi, S.-X., Xi, S.-Q., Yu, H., et al. 2016, ApJS, 224, 20
Yuan, Q., Wang, Q. D., Liu, S., & Wu, K. 2018, MNRAS, 473, 306
Zhang, H.-M., Wang, Z.-J., Zhang, J., et al. 2020, PASJ, 72, 44
Zhang, H.-M., Zhang, J., Lu, R.-J., et al. 2018, RAA, 18, 040
Zhang, J., Sun, X.-N., Liang, E.-W., et al. 2014, ApJ, 788, 104
Zhang, W.-L., Yi, S.-X., Yang, Y.-P., & Qin, Y. 2022, RAA, 22, 065012